Characterization of a highly neutralizing single monoclonal antibody to botulinum neurotoxin type A

Sébastien Brier, Christine Rasetti-Escargueil, Anne Wijkhuisen, Stéphanie Simon, Maud Marechal, Emmanuel Lemichez, Michel Popoff

CHARACTERIZATION OF A HIGHLY NEUTRALIZING SINGLE MONOCLONAL ANTIBODY TO BOTULINUM NEUROTOXIN TYPE A

Sébastien Brier[1], Christine Rasetti-Escargueil[2], Anne Wijkhuisen[3], Stéphanie Simon[3], Maud Marechal[2], Emmanuel Lemichez[2], Michel R. Popoff[2*]

[1]Biological NMR Technological Plateform, Institut Pasteur, CNRS UMR3528, 75015 Paris, France

[2]Institut Pasteur, Toxines Bactériennes, CNRS ERL6002, 75015 Paris, France

[3]Université Paris-Saclay, CEA, INRAE, Département Médicaments et Technologies pour la santé, 91191 Gif-sur-Yvette, France

- Corresponding author popoff2m@gmail.com, Ph 33 643551035

ABSTRACT (228 mots)

Compared to conventional antisera strategies, monoclonal antibodies (mAbs) represent an alternative and safer way to treat botulism, a fatal flaccid paralysis due to botulinum neurotoxins (BoNTs). In addition, mAbs offer the advantage to be produced in a reproducible manner. We previously identified a unique and potent mouse mAb (TA12) targeting BoNT/A1 with high affinity and neutralizing activity. In this study, we characterized the molecular basis of TA12 neutralization by combining Hydrogen/Deuterium eXchange Mass Spectrometry (HDX-MS) with site directed mutagenesis and functional studies. We found that TA12 recognizes a conformational epitope located at the interface between the H_{CN} and H_{CC} subdomains of the BoNT/A1 receptor-binding domain (H_C). The TA12 binding interface shares common structural features with the ciA-C2 VHH epitope and lies on the face opposite recognized by ciA-C2 and the CR1/CR2 neutralizing mAbs. The single substitution of N1006 was sufficient to affect TA12 binding to H_C confirming the position of the epitope. We further uncovered that the TA12 epitope overlaps with the BoNT/A1 binding site for both the neuronal cell surface receptor synaptic vesicle glycoprotein 2 isoform C (SV2C) and the GT1b ganglioside. Hence, TA12 potently blocks the entry of BoNT/A1 into neurons by interfering simultaneously with the binding of SV2C and to a lower extent GT1b. Our study reveals the unique neutralisation

mechanism of TA12 and emphasizes on the potential of using single mAbs for the treatment of botulism type A.

Key Words

Botulinum neurotoxin; Botulism; Monoclonal antibody; Synaptic vesicle protein 2; GT1b, Mass spectrometry; Hydrogen-Deuterium eXchange; Epitope mapping

Running title

Potent neutralization of BoNT/A1 with a single mAb

Nonstandard abbreviations

BoNT, botulinum neurotoxin
L, light chain
H, heavy chain
H_C, half C-terminal H chain
H_N, half N-terminal H chain
SV2C, synaptic vesicle protein 2C
gSV2C, glycosylated SV2C
SNARE, soluble *N*-ethylmaleimide-sensitive-factor attachment protein receptor
mAb, monoclonal antibody
HDX-MS, Hydrogen/Deuterium eXchange Mass Spectrometry
TCEP, Tris(2-carboxylethyl)phosphine
EIA, enzyme immunoassay
LD, luminal domain
BSA, bovine serum albumin
AMC, anit-mouse Fc
TGY, trypticase-glucose-yeat extract
VHH, variable domain of heavy chain
MLD, mouse lethal dose

INTRODUCTION

Botulism is a rare but severe disease that results from botulinum neurotoxin (BoNT) intoxication. Naturally acquired botulism can develop in three main forms: foodborne BoNT intoxication, intestinal colonization by BoNT-producing clostridium (infant botulism and more rarely botulism by intestinal colonization in adults), or wound botulism. Among the seven different BoNT toxinotypes, BoNT/A is the most potent toxin with a lethal dose for human estimated at ~1 ng/kg by parenteral route (1, 2). BoNTs and specially the BoNT/A toxinotype are therefore classified by the Centers for Diseases Control and Prevention (CDC) among the six major bioterrorism agents (category A) (3). BoNT/A is a ~1296 residues long protein that is proteolytically processed into a light (L) and a heavy chain (H) linked by a single disulfide bond. The L chain contains the intracellularly active enzymatic site that specifically cleaves neuronal members of the *N*-ethylmaleimide sensitive factor attachment protein receptors (SNAREs) complex required for the release of acetylcholine. The C-terminal H chain (H_C) recognizes both the intraluminal loop of the synaptic vesicle glycoprotein 2C (SV2C) and GT1b/GD1a gangliosides as functional dual receptors on neuronal cells. Finally, the N-terminal H domain (H_N) is involved in the translocation of the L chain from endocytic vesicles into the cytosol of neuronal cell targets (4-11).

Antitoxin serotherapies are currently the only specific and available treatments for botulism. The clinical benefit and effectiveness of such therapies remain however linked to their use at the early onset of the disease *only*. The equine antitoxin therapy composed of polyclonal IgG antibodies is the most available treatment although it is often associated to hypersensitivity reactions including serum sickness and cardiac arrest (12, 13). Human botulism-immune globulins from vaccinated donors have been developed notably for the treatment of infant botulism (14). The first one—BabyBIG, is supplied by the California Department of Public Health, but with limited stock. This formulation has been recently discontinued and will be replaced with a new formulation currently under clinical development (15). Recently, the safety of a new cocktail composed of three humanized mAbs (XOMA 3B) engineered to neutralize BoNT/A subclasses has been evaluated and confirmed in healthy volunteers (16). The European AntiBotABE Program has allowed the isolation of recombinant humanized antibodies neutralizing BoNT/A, B and E. Protective antibody combinations against BoNT/A and BoNT/B showed cross-neutralization of both BoNT/A1 and A2 as well as BoNT/B1 and B2, repectively (17).

Monoclonal antibodies (mAbs) represent therefore a promising alternative strategy to treat botulism with the advantage of being better tolerated by patients and produced in a more

reproducible and safer way than animal hyperimmune serum. Various murine or humanized mAbs raised against whole BoNTs or BoNT subdomains have been evaluated for their neutralizing potency and their possible therapeutic use (review in (17, 18)). Most often, efficient toxin neutralization requires a combination of several mAbs. For example, the association of three mAbs has been reported to neutralize BoNT/A, BoNT/E, or BoNT/F, respectively (19-21). Recently, a single anti-BoNT/A tri-epitopic mAb with equivalent binding and neutralization potency than three distinct mAbs has been generated (22). The use of a single mAb as alternative therapeutic antitoxin agent appears therefore promising and offers the advantage to simplify the process of development and to reduce the cost of production.

We previously reported a potent neutralizing murine mAb (named TA12) generated against the C-terminal domain of the BoNT/A1 heavy chain (H_CA1) (23, 24). In this study, we focused on the structural characterization of the TA12:H_CA1 complex by Hydrogen/Deuterium eXchange Mass Spectrometry (HDX-MS) approach combined with site directed mutagenesis and functional assays (25, 26). We report that TA12 targets a conformational epitope on H_CA1 located at the junction between the H_{CC} and the H_{CN} subdomains. The TA12 epitope overlaps with both the SV2C cell receptor and the GT1b binding sites, hence perturbing the dual-receptor binding process required for the entry of BoNT/A1 into neuronal cells.

MATERIALS AND METHODS

Biological reagents

mAb TA12 was prepared and affinity purified on protein A beads (Prosep-A High capacity, Millipore, Billerica, USA) as previously described (27).

Recombinant H_C of BoNT/A1 (H_CA1), corresponding to the receptor binding domain of BoNT/A1 was prepared as previously described (28). DNAs encoding H_C of BoNT/A subtypes were PCR amplified with primers and *C. botulinum* genomic DNA (**Extended Table 1**) and cloned into pET28a. Recombinant H_C containing N-terminal 6xHis-tag were produced and purified as previously described (28). Primers used to generate H_CA1 mutants are indicated in **Extended Table 2**.

cDNA encoding the human intraluminal SV2C fragment L4 (amino acid 454 to 579, hereafter named SV2C-LD) was PCR amplified as previously described (29). Briefly, DNA encoding the amino acids 454 to 579 of human SV2C was PCR amplified with primers P1415 (5'- GGATCCTTCCCTGATGTCATTAAACCTCTG-3') and P1416 (5'- GAATTCCTAGTAGGCACTATAGTCATCATCAAA-3') adding *Bam*HI and *Eco*RI restriction sites, respectively, and was cloned into pGEX-2T at the corresponding restriction

sites. The construction was verified by DNA sequencing. The fusion protein (41 kDa) contains N-terminal GST and C-terminal SV2C-LD linked by Gly-Ser resulting from the *Bam*HI site. The recombinant plasmid was cloned into *E. coli* BL21 DE3 and the resulting bacterial strain was grown in LB medium containing ampicillin (100 µg/ml). The culture was induced with IPTG (0.2 mM) and further grown at 18°C for 18 h. The bacterial cells were washed with distilled water, suspended in 50 mM Tris, 150 mM NaCl, 10 mM $MgCl_2$, 1 mM dithiotreitol, 0.1% Tween20 containing complete protease inhibitor cocktail EDTA free (Roche, France), and lyzed by ultrasonication. The lysate was incubated with Glutathione-Sepharose-4B beads (GE Healthcare) for 1 h at 4°C. The beads were washed three times with the same buffer and a 50% suspension in the same buffer was used for the pull-down assays.

For HDX-MS experiments, 6His-tag-SV2C-LD was used. The PCR amplified DNA encoding SV2C-LD was cloned into pET28 vector at the *Bam*HI-*Eco*RI site. The recombinant N-terminal 6His-tag-SV2C-LD protein was produced in *E. coli* BL21 DE3 and purified on a Talon metal affinity matrix (Clontech) equilibrated in 10 mM Tris, 150 mM NaCl, 10 mM imidazole, 10 mM TCEP, pH 7.5. The recombinant protein was eluted with the same buffer supplemented with 100 mM imidazole and dialyzed against the same buffer without imidazole.

Affinity determination of mAb TA12

The affinities of mAb TA12 for different recombinant H_CBoNT isoforms were determined by Bio-layer Interferometry using the ForteBio system (Pall Laboratory). mAb TA12 prepared at 10 µg/mL in EIA (enzyme immunoassay) buffer (0.1 M phosphate buffer, pH 7.4, 0.15 M NaCl, 0.1% BSA, and 0.01% sodium azide) + 0.02% Tween 20 (Sigma) was dispensed in 96-well microplates at a volume of 200 µL per well. The same concentration occupied 8 vertical wells. In other wells, recombinant H_CBoNT proteins were dispensed at 8 titrated concentrations (between 100 and 0 nM depending on the protein). A glycine (Sigma, pH [1.4]) regeneration solution and EIA buffer + 0.02% Tween 20 for baseline stabilization and neutralization was also prepared. The plate was agitated at 1000 rpm over the entire course of the experiment. Prior to the binding measurements, the anti-mouse Fc (AMC) sensors tips were hydrated in EIA buffer + 0.02% tween 20. The sensor tips were then transferred to the EIA buffer + 0.02% Tween 20 for the baseline, then for 300 sec into wells containing mAb for loading step. After baseline step in EIA buffer + 0.02% Tween 20 for 60 sec, the binding kinetics were measured by dipping the mAb-coated sensors into the wells containing recombinant H_CBoNT at varying concentrations. The binding interactions were monitoring over a 900 sec associated period and followed by a 900 sec dissociation period in the wells containing EIA buffer +0.02 % Tween

20. Between each binding cycle, the AMC sensors tips were regenerated with wells containing glycine and neutralized in the EIA buffer + 0.02% tween 20. The equilibrium dissociation constant (K_D) was calculated using the ratio between the dissociation rate constant (k_{off}) and the association rate constant (k_{on}), obtained with a global Langmuir 1:1 fit (Octet Data Analysis software, vHT.10).

GST pull down assay

Recombinant SV2C-LD immobilized on glutathione-Sepharose-4B matrix (GE healthcare, France) (30 µL of 50% bead suspension) was incubated for 90 min at 4°C with H_CA1 solutions prepared with or without mAb TA12 in 50 mM Tris buffer, 150 mM NaCl, 10 mM $MgCl_2$, 2 mM dithiothreitol, 0.1% Tween 20, pH 7.5, supplemented with antiproteases (protease inhibitor cocktail EDTA free, Roche Diagnostics, Germany) (final volume 400 µL). H_CA1:TA12 solutions were pre-incubated for 15 min at room temperature before use. Beads were collected by centrifugation and washed three times with the same buffer. Washed pellets were suspended in SDS/2-mercaptoethanol sample buffer for 2 min at 95°C and analyzed by SDS-PAGE. Proteins were stained by Coomassie blue.

Ganglioside binding assay

Binding of H_CA1 to the GT1b ganglioside was assessed in a solid phase assay as previously described (30-32). Briefly, bovine brain GT1b (Calbiochem, France) stored in dimethyl sulfoxide (20 mg/mL) at -20°C was diluted in methanol and applied overnight to 96-well plates (Corning-Costar, France) at 2 µg per well. Methanol was evaporated at room temperature and the plates were washed three times with phosphate-buffered saline containing 0.05 % Tween 20 (Sigma, France) (PBST). Plates were blocked with 5% non-fat skim milk in PBST for 1 h at room temperature and washed with PBST. H_CA1 was then dispensed (10 nM/well in PBS) in the control wells and incubated for 2 h at 4°C. For competition with mAb TA12, H_CA1 (10 nM) was incubated with various concentrations of TA12 in 100 µL PBS for 15 min at room temperature prior being applied to GT1b coated wells for 2 h at 4°C. After washing with PBST, bound H_CA1 was detected with rabbit anti-H_CA1 (1:10,000) (29) and horse radish peroxidase (HRP) goat anti-rabbit immunoglobulin IgG (1:3,000) (Invitrogen, France). Ortho phenylendiamine (Sigma, France) was used as substrate (1 mg/mL in citrate buffer pH 4.5 containing H_2O_2), and the reaction was stopped with HCl 3 M (50 µL/well). The extinction was measured at 490 nm and 650 nm as reference.

198

199 **Neutralizing activity**

200 BoNTs were prepared from *C. botulinum* cultures in TGY (trypticase-glucose-yeast
201 extract) medium for four days under anaerobic conditions at 37°C as previously described (33).
202 Briefly, the cultures were acidified at pH 3.5 with sulfuric acid, centrifuged at 10,000 x g for
203 15 min at 4°C, washed with distilled water, and the BoNT complexes were extracted three times
204 with 0.2 M phosphate buffer pH 6.3. BoNT complexes were precipitated with 65% ammonium
205 sulfate saturation and then dialyzed against 50 mM phosphate buffer, pH 6.3 containing 0.2%
206 gelatin (PB-G).

207 Mouse protection assay was performed with male Swiss mice (Charles River) weighing
208 20-22 g as previously described (34). Variable amounts of TA12 were incubated with 5
209 estimated mouse 50% lethal doses of either BoNT/A1, A2, A3, A5 or A7 in PB-G for 30 min
210 at room temperature. The mixtures (0.5 mL) were then injected intraperitoneally into mice with
211 control mice receiving BoNT alone. Mice were observed and any death was recorded every day
212 during 4 days.

213

214 **Ethic statements**

215 All experiments were performed in accordance with French and European Community
216 guidelines for laboratory animal handling. The protocols of experiments were approved by
217 Institut Pasteur CETEA (Comité d'Ethique en Expérimentation Animale) with the agreement
218 of laboratory animal use (N° 2013-0116) and by the Ministère de l'Education Nationale et de
219 l'Enseignement Supérieur with the agreement 02026.02.

220

221 **HDX-MS experiments**

222 A summary of the HDX data containing the main experimental details is provided in
223 **Extended Table 3** (35). Prior to initiating the labeling, the quality of each protein was assessed
224 by SDS-PAGE and intact mass analysis (**Extended Figure 1**).

225

226 ***Sample preparation.*** For epitope mapping, H_CA1 was labeled in both the presence and absence
227 of the mouse mAb TA12. The TA12: H_CA1 complex was formed by mixing 3 µL of H_CA1 (29
228 µM in buffer A: 10 mM Tris, 150 mM NaCl, pH 7.4) with 4.5 µL of mAb TA12 (27 µM in
229 buffer A). Control samples (unbound H_CA1) were prepared in parallel by replacing TA12 with
230 buffer A. After 1 h incubation at 20°C, the labeling was initiated by adding 67.5 µL of

deuterated buffer (10 mM Tris, 150 mM NaCl, pD 7.4; D_2O/H_2O ratio: 90/10%). Assuming a K_D value of ~20 pM (24) (and this study), ~100% of H_CA1 remains bound to TA12 during hydrogen exchange. Continuous labeling was performed at 20°C for t = 0.16, 1, 5, 10, 30, 60 and 120 min. Aliquots of 10 µL (*i.e.,* 11.6 pmoles of H_CA1) were removed and quenched upon mixing with 50 µL of an ice cold solution of 2% formic acid, 4M urea to decrease the pH to 2.5 (Final D_2O/H_2O ratio: 15/85%). Quenched samples were immediately snap frozen in liquid nitrogen and stored at -80°C until MS acquisition (less than 3 days).

An identical procedure was used to map the SV2C-LD interaction site on H_CA1. The SV2C-LD: H_CA1 complex was formed by mixing 3 µL of H_CA1 (29 µM in buffer A) with 4.5 µL of SV2C-LD (22 µM in buffer A supplemented with 10 mM TCEP). The labeling was performed in the presence of 1 mM TCEP at 20°C. Assuming a K_D value of 28 nM (6), 90.5% of H_CA1 remains bound to SV2C-LD during labeling.

Undeuterated H_CA1 samples were obtained following the same experimental procedure. A fully deuterated H_CA1 control was prepared in 10 mM Tris buffer, 150 mM NaCl, 8 M urea-d4, pD 7.4 (D_2O/H_2O ratio: 90/10%), incubated overnight at 20°C and processed as described above. All samples were prepared in triplicate for each time point and condition (independent technical replicate).

Data acquisition. Quenched samples were rapidly thawed and injected onto a nanoACQUITY UPLC M-Class system (Waters Corporation, Milford, MA) equipped with a HDX manager maintained at 0°C to minimize back-exchange. Labeled samples (9.7 pmol of H_CA1 either alone or with 13.5/11 pmol of TA12/SV2C-LD) were digested using an in-house packed cartridge (2.0 x 20 mm, 63 µL bed volume) of immobilized pepsin beads (Thermo Scientific, Rockford, IL) for 2 min at 20°C. Peptides were directly trapped and desalted onto a C18 Trap column (VanGuard BEH 1.7 µm, 2.1 x 5 mm, Waters Corporation, Milford, MA) at a flow rate of 100 µL/min (0.15% formic acid) and separated by a 10 min linear gradient of 5-40% acetonitrile at 40 µL/min using an ACQUITY UPLC BEH C18 analytical column (1.7 µm, 1 × 100 mm, Waters Corporation, Milford, MA). After each run, the pepsin column was manually cleaned with two consecutive injections of 1% formic acid, 5% acetonitrile, 1.5 M guanidinium chloride, pH 1.7. Blank injections were performed between each run to confirm the absence of carry-over. Mass spectra were acquired in resolution and positive mode (*m/z* 50-2000) on a Synapt G2-Si HDMS mass spectrometer (Waters Corporation, Milford, MA) equipped with a standard ESI source and lock-mass correction. Peptic peptides were identified in undeuterated

samples by a combination of data independent acquisition (MS^E) and exact mass measurement (below 5.0 ppm mass error) using the same chromatographic conditions than for the deuterated samples.

Data processing. The initial peptide map of H_CA1 was generated by database searching in ProteinLynX Global server 3.0 (Waters corporation, Milford, MA) using the following processing and workflow parameters: low and elevated intensity thresholds set to 100.0 and 50.0 counts; intensity threshold sets to 750.0 counts; automatic peptide and fragment tolerance; non-specific primary digest reagent; false discovery rate sets to 4%. Each fragmentation spectrum was manually inspected for assignment confirmation. The peptide map was refined in DynamX 3.0 (Waters corporation, Milford, MA) using the following Import PLGS results filter: minimum intensity = 1500; minimum products per amino acid = 0.4; minimum score = 6.8; maximum MH+ error (ppm) = 5; file threshold = 2.

DynamX 3.0 was used to extract the centroid masses of all peptides selected for HDX-MS analyses. Only one unique charge state was considered per peptide and no back-exchange correction was performed. HDX results are reported as relative deuterium exchange level expressed in either mass unit or fractional exchange. Fractional exchange data were calculated by dividing the experimental uptake value by the theoretically maximum number of exchangeable backbone amide hydrogens that could be replaced into each peptide in 90% excess deuterium. MEMHDX (36) was used to visualize and statistically validate the HDX data (Wald test, false discovery rate of 5%).

The presence of bimodal *m/z* envelopes (i.e., EX1 behavior) was determined by visually inspecting the shape of the isotopic distribution for all peptides. HX-Express2 software was used to extract the uptake value of bimodal *m/z* envelopes using a Double-Gaussian fitting (37).

RESULTS

TA12 efficiently neutralizes BoNT/A1

BoNT/A is divided into 8 distinct subtypes (BoNT/A1 to BoNT/A8) according to their amino acid sequence variations ranging from 2.9 % to 15.6 % (1). Although the BoNT/A toxinotype is defined by its neutralization with polyclonal anti-BoNT/A antibodies, each subtype can be distinctly neutralized by individual mAbs (1). We recorded that TA12 efficiently neutralized BoNT/A1 and displayed an inhibitory spectrum on BoNT/A subtypes A2, A3, and A7 (**Table 1**) (23). However, it showed a weak neutralizing activity against BoNT/A5 (**Table 1**). Taken together, these results confirm that TA12 is a highly neutralizing mAb of the most

potent subtype BoNT/A1 with medium neutralizing activity against BoNT/A2 and A3 subtypes and low neutralizing activity against BoNT/A5 (38, 39).

TA12 binding affinity to BoNT/A subtypes

TA12 binding affinity to the H_C domain of different BoNT/A subtypes was determined by Bio-Layer Interferometry. The binding affinity of TA12 was very high for H_CA1, H_CA2, and H_CA3 with K_D values in the low pM range (i.e., < 100 pM; **Table 2**) in good agreement with previous data obtained for H_CA1 using Biacore instrument (24). The TA12 affinity was slightly lower with H_CA2 and significantly reduced with H_CA4, H_CA5, and H_CA7 with K_D values in the low nM range. These differences in K_D mainly result from faster dissociation rate values for H_CA2, H_CA4, H_CA5, and H_CA7 as compared to H_CA1. Indeed, TA12 interacts with the H_C domain of the different BoNT/A subtypes with similar on-rates values (**Table 2**). Consistent with the protection of TA12 on BoNT/A subtypes, TA12 binds BoNT/A Hc domains with maximal affinities for BoNT/A1, A2, and A3. These results reveal that low picomolar affinities for the H_C domain are required to achieve maximal TA12 neutralizing power in the mouse lethality assay.

TA12 recognizes a conformational epitope at the junction between the H_{CC} and the H_{CN} subdomains of H_CA1

To better understand the mechanism underlying BonT/A1 neutralization by TA12, the free and TA12-bound state of H_CA1 were subjected to HDX-MS analysis. The quench and pepsin digestions were first optimized to generate a peptide map with high sequence coverage and peptide redundancy. Urea was included in the quench buffer to favor the dissociation of the TA12: H_CA1 complex and increase the accessibility of both proteins to pepsin during the digestion step. A total of 98 unique peptides covering 85.2% of the H_CA1 sequence were confidently identified, of which 62 were selected for HDX-MS (**Extended Figure 2**). Overlapping peptides were only used to increase the spatial resolution when their back-exchange values were similar (i.e., < 10%; **Extended file HDX.xls**).

The binding of TA12 reduces the solvent accessibility of 12 peptides covering six distinct regions within H_CA1 (**Figure 1A, Extended Figure 3**). The main decreases in solvent accessibility occur in region 2 (peptide 1005-1016; loop β31-β32, β32), in region 4 (peptides 1114-1134, 1115-1134, 1116-1134 and 1117-1134; loop-β38-loop), and in region 5 (peptides 1135-1144, 1135-1147 and 1148-1154; β39-loop-β40-loop-β41). Inspection of the different

overlapping peptides in regions 2 and 4 reveals that the reduction of solvent accessibility is restricted to segments 1005-1009 and 1116-1124. In addition, a slight but statistically significant reduction in solvent accessibility was observed in region 1 (peptides 946-955, 946-958 and 946-961; loop β27-β28) and in region 6 (peptide 1250-1261; β49-loop) (**Figure 1A and Extended Figure 4A**).

As shown in **Figure 1B**, TA12 binds H_CA1 at the junction between the N-terminal lectin subdomain (H_{CN}) and the C-terminal trefoil subdomain (H_{CC}). The TA12 epitope appears conformational and mainly formed by the β27-β28 and β31-β32 loops of H_{CN} and by the structural elements β38 to β41, β49 and the β37-β38, β39-β40, β40-β41 and β49-β50 loops of H_{CC}. Interestingly, the HDX-MS defined TA12 epitope contains elements identified as important for the binding of both the SV2C luminal domain (SV2C-LD) and the GT1b ganglioside (**Figure 1B, regions 4, 5 and 6**). Indeed, the SV2C-LD binding site has been characterized in the H_{CN}-H_{CC} interface and the ganglioside binding pocket in the C-terminal part of H_{CC} (Glu1203-Gly1279 with Tyr1117 and Phe1252 playing a critical role) (6, 9, 40). Finally, TA12 also increases the deuterium uptake in region 3 (peptide 1017-1035; β32-loop-β33) in the lectin subdomain (**Figures 1A, 1B**). Upon complex formation, the isotopic profile of peptide 1017-1035 adopts a bimodal distribution characterized by a low and high *m/z* protein population (**Figure 1C**). Bimodal isotopic patterns result from cooperative exchanges (also known as EX1 regime) and are very rare in proteins under physiological conditions. Several experimental factors, such as carry-over or abnormal gas-phase back-exchange are known to generate false EX1 signatures. To rule out these possibilities, a blank was acquired between each injection and the pepsin column was carefully washed after each run. In addition, specific settings were applied on the mass spectrometer (source and ion transfer) to prevent gas-phase deuterium loss (41). We are therefore confident that the bimodal pattern observed with peptide 1017-1035 is not an experimental artefact but a true change in dynamics imposed by the binding of TA12. To extract the deuterium uptake level of the low and high *m/z* protein populations, the bimodal isotopic envelop was fitted with two Gaussians. The low *m/z* population showed no difference in deuterium uptake compared to free H_CA1 (**Figure 1C**). The high *m/z* population however displayed an evident and constant increase in deuterium uptake over time, with the incorporation of four additional deuteriums. This data confirms that segment 1017-1035 is destabilized in the complex.

Taken together, these data reveal that TA12 targets a conformational epitope located at the junction between the H_{CN} and H_{CC} subdomains that overlaps with the the SV2C-LD and the

GT1b binding site. The formation of the complex triggers a conformational change in the H_{CN} domain that was not observed with the two previously described neutralizing antibodies ciA-C2 and CR1 (see discussion) (42-45).

TA12 prevents BoNT/A1 interaction with SV2C-LD

The HDX-defined TA12 epitope overlaps with the SV2C-LD and the GT1b binding sites identified by X-ray crystallography (6, 40). SV2C-LD and GT1b both correspond to the neuronal cell surface receptors used by BoNT/A to efficiently and specifically enter neurons via a synergetic dual-binding process (8, 46-48). Based on this observation, we hypothized that TA12 binding might interfere with the interaction of both SV2C-LD and GT1b.

We first focused our attention on the H_CA1:SV2C-LD interaction. The deuterium uptake profil of H_CA1 was monitored in the SV2C-LD:H_CA1 complex and compared to the one obtained in the presence of TA12. The binding of SV2C-LD induced several statistically significant changes (Wald test, $p<0.05$) in deuterium uptake in H_CA1 (**Figure 2A; Extended Figures 4B, 5**). As observed in the H_CA1:TA12 complex, major reductions were observed in region 2 of the H_{CC} domain (peptides 1145-1154 and 1148-1154, region 5 in **Figure 1**) covering loops β39-β40 and β40-β41. Region 2 corresponds to the main SV2C-LD interaction site identified by X-ray crystallography and contains critical residues for binding such as T1145 and T1146 (**Figures 2B**) (6, 10). Therefore, these data confirm that TA12 and SV2C both target a common binding region on H_CA1 (Compare **Figures 1A, 1B and 2A, 2B**). Two additional regions surrounding residues 1145-1154, namely region 1 (peptides 946-955, 946-958 and 946-961) in the H_{CN} domain and region 3 (peptides 1282-1296, 1283-1296, 1284-1296 and 1285-1296) in the C-terminal part of H_{CC}, also display minor but statistically significant reductions in uptake upon complex formation. Region 3 contains several overlapping peptides with similar back-exchange values (**Extended file HDX.xls**) allowing to confine the effects of SV2C-LD binding to segment 1285-1296 *only*. This segment contains residue R1294 involved in the interaction and the binding specificity with SV2C-LD. Finally, although region 1 is very close to the main SV2C-LD interaction site (i.e., region 2), this latter was not identified as part of the SV2C-LD binding interface by X-ray crystallography (**Figure 2B**). Based on this observation, the slight decrease in solvent accessibility observed in 946-961 might be attributed to a change in dynamics rather than a masking effect.

We next performed *in vitro* experiments to analyze the interference of TA12 on the binding of recombinant H_CA1 to SV2C-LD immobilized on glutathione-Sepharose 4B beads. As shown in **Figure 2C**, H_CA1 binding to immobilized SV2C-LD was prevented in a TA12 dose-

dependent manner. More than 90% inhibition of binding was obtained at an equimolar ratio between TA12 and H_CA1. These results confirm that TA12 prevents the formation of the toxin/receptor complex via direct interaction with H_CA1. Thus, as observed with the neutralizing ciA-C2 VHH, TA12 blocks the entry of BoNT/A1 into neuronal cells by targeting one critical area of the toxin-cell receptor interface.

TA12 affects H_CA1 binding to GT1b

We next focused our attention on the H_CA1:GT1b interaction. Our HDX-MS data shows that TA12 affects the solvent accessibility of elements involved in the GT1b-binding site (**Figure 3A**). Region 1116-1124 contains residue Y1117 which directly coordinates GT1b through hydrogen bondings with sialic acid 5 (Sia5); residue F1252 in region 1250-1252 also hydrogen bonds to galactose 4 (Gal4) of the GT1b ganglioside (40). Compared to SV2C-LD, GT1b only shares a limited overlapping binding area with TA12 on H_CA1 (**Figure 3A**). Therefore, TA12 is not expected to directly compete with GT1b binding on H_CA1 as observed with SV2C-LD but rather to affect the H_CA1:GT1b interaction mainly through steric clashes.

To determine the effects of TA12 on H_CA1 binding to GT1b, an inhibition binding assay was performed using GT1b coated on plastic plate and incubated with H_CA1 either alone or in the presence of TA12. A shown in Figure 3B, increased concentrations of TA12 result in inhibition of H_CA1 binding to GT1b. Complete inhibition of H_CA1 binding to GT1b was achieved at a much higher TA12/H_CA1 molar ratio compared to SV2C-LD (10:1 for GT1b; 1:1 for SV2C-LD), hence suggesting that TA12 mainly causes indirect interferences with GT1b. Altogether, these data confirm that TA12 is also able to interefere with H_CA1 binding to GT1b abeit with a lower efficiency compared to the binding inhibition of HcA1 to SV2C-LD.

Residue N1006 is important for TA12 binding.

Although TA12 recognizes the H_C domain of BoNT/A subtypes with high affinity (i.e., in the low pM-nM range; **Table 2**), the efficiency of neutralization appears subtype dependent. The quantity of TA12 required to neutralize 50% of the activity of both BoNT/A5 and A7 appears 400- and 40-fold higher than for BoNT/A1, respectively (**Table 1**). Interestingly, the H_C domain of BoNT/A1 shares respectively 94.1 and 91.7% sequence identity with H_CA5 and H_CA7, suggesting that small variations in the primary sequence are sufficient to explain the difference of neutralizing potency by TA12. To test this hypothesis, specific residues mainly positioned within the HDX-MS defined TA12 epitope where major changes in deuterium uptake occur upon binding were selected for substitution (**Extended Figure 6**). Four distinct

residues of H_CA1 including N1006 (region 2, **Figure 1**), and V1143, M1144 and R1156 (region 5, **Figure 1**) were replaced by the corresponding residues found in H_CA5 or H_CA7. The modified residues correspond to natural H_C variants and their mutation is therefore not expected to cause any local secondary structural changes on H_CA1. The substitution of V1143 alone or in combination with M1144 and R1156 showed no significant effect on TA12 binding (**Table 2**). By contrast, the substitution of N1006 with alanine strongly affects the binding of TA12 to H_CA1 with a 280-fold reduction in affinity compared to wild type (**Table 2**) confirming the importance of N1006 in complex formation.

DISCUSSION

Neutralizing antibodies against BoNT represent the only available antidote against botulism considering that vaccination is not an appropriate strategy due to the expanding therapeutic applications of BoNTs. Although equine anti-BoNT polyclonal sera are able to efficiently neutralize all seven known BoNT toxinotypes, their use can cause dramatic side effects (13, 49-53). Alternative therapeutic antitoxin approaches, such as mAbs or peptide inhibitors (6), are currently explored to reduce the risks of serum sickness and cardiac arrest. Human anti-BoNT immune globulins obtained from vaccinated donors have been developed for the treatment of infant botulism, but their production is not easily scalable (14). Recombinant mAbs and more specially recombinant humanized mAbs represent a promising and safer alternative strategy for botulism treatment. Their production is highly reproducible compared to animal hyperimmune sera thereby preventing batch to batch variations in antibody affinity (50). Over the last decade, several neutralizing mAbs against the distinct BoNT types have been generated (17, 18, 54). However, mAbs are specific of single epitopes *only* and extended protective coverage most often requires the combination of several mAbs. For example, the association of three distinct mAbs targeting non-overlapping epitopes of BoNT/A was found to be highly protective, whereas each single mAb showed no significant protection. Moreover, the three mAb in combination induced a 90-fold greater neutralizing potency of BoNT/A than human hyperimmune globulins (21). Altough effective to treat botulism, the association of several mAbs introduces unique development and manufacturing challenges for clinical application. Recentlty, a single tri-epitopic IgG1-based mAb (TeAb) containing the binding sites of three individual anti-BoNT/A1 mAbs was engineered (22). TeAb was found to be much more potent in mouse-neutralization assay than any of the three single mAbs and almost as potent as the combination of the three individual mAbs against BoNT/A1. Though

the neutralization potency of TeAb against the other BoNT/A subtypes was not reported, this work highlights the potential of using single mAbs as alternative antitoxin solution (22).

In this study, we showed that the single TA12 mAb raised against H_CA1 is a potent inhibitor of the two most frequent subtypes involved in human botulism, namely A1 and A2 (55-57), but also A3. TA12 recognizes a conformational epitope mainly composed of solvent accessible loops located at the interface between the H_{CN} and the H_{CC} subdomain. The TA12 binding site overlaps with both the SV2C and the GT1b binding interfaces on H_CA1, causing interferences with the interaction of the two neuronal cell surface receptors used by BonT/A to enter neutrons. The strong neutralization potency of TA12 is therefore achieved by the synergetic and simultaneous inhibition of BoNT/A binding to GT1b and the peptide moiety of the SV2C luminal domain.

Two additional BoNT/A neutralizing antibodies have been reported to block the recognition of SV2C: the camelid single domain ciA-C2 antibody (42, 43) and the human monoclonal antibody CR1 currently in clinical trials (44, 45). The identification of the TA12 binding site provides a means to compare the different epitopes on H_CA1 and the neutralization mechanism of each antibody. All three antibodies target the same H_{CN}/H_{CC} junction, which was shown to elicit neutralizing antibodies against BoNT/A (28), but they adopt distinct orientation on H_CA1 (**Figure 4**). CR1 mainly occupies the SV2C glycan binding site on the H_{CN} subdomain. The CR1 epitope locates on the same H_CA1's face than the glycosylated SV2C (gSV2C) without sharing any overlapping peptide regions with gSV2C. The large size of CR1 and its close proximity with gSV2C are sufficient to generate local steric clashes between portions of CR1 and gSV2C, causing indirect interferences with gSV2C binding on H_CA1 (10, 45). The strong neutralizing potency of CR1 is therefore driven by two simulatenous blocking effects: an indirect effect with the SV2C peptides moieties and a direct effect through the occupation of the SV2C glycan binding site. As observed with CR1, ciA-C2 largely occupies the binding site for the SV2C glycan but it also interacts with a key region in the H_{CN} subdomain containing critical residues for gSV2C binding (**Figure 4**). Thus, ciA-C2 simulatenously inhibits both the protein- and the glycan- interactions between BonT/A1 and gSV2C via direct blocking effects (43). The TA12 epitope shares common structural features with ciA-C2 as they both occupy the same gSV2C peptide binding site on H_CA1 and directly block gSV2C binding to BoNT/A (**Figure 4**). However, the TA12 binding interface lies on the face opposite recognized by both ciA-C2 and CR1, confirming that the H_{CN}/H_{CC} junction contains distinct antigenic regions able to elicit highly potent and unique BoNT/A neutralizing antibodies (28).

In contrast to both ciA-C2 and CR1, TA12 does not compete with the SV2C glycan but interferes with H_CA1 binding to GT1b.

The identification of the TA12 epitope on BoNT/A also provides a means to understand the variations in potency observed with the different H_CA subtypes (**Tables 1, 2**). The three main regions defining the TA12 epitope (i.e., I1005-D1009, Y1117-V1125, and L1136-L1154; **Extended Figure 6**) are relatively well conserved hence explaining the capabilities of TA12 to recognize all H_CA subtypes with high affinity. As previously reported, the antitoxin efficacy of antibodies largely depends on their binding affinity (42). Thereby, the highest TA12 binding affinities and neutralization potencies were obtained with subtypes A1, A3 and A2 whereas the lowest were observed with A5 and A7. TA12 binds A5 and A7 with affinity values comparable to both ciA-C2 and CR1 (i.e, in the low nanomolar range), and yet only poorly neutralizes BoNT/A5 in the mouse lethality assay. Low nanomolar K_D are therefore not sufficient because TA12 interferes simultaenously with the two BoNT/A cell binding partners. The unique neutralization mechanism of TA12 requires therefore low picomolar range affinity to prevent the deplacement of the bound antibody from the toxin by either gSV2C, GT1b or both. We believe therefore that the differences in potency observed between H_CA subtypes are due to subtle amino-acid changes within the TA12 binding interface, resulting in lower K_D values, as we showed with residue 1006 in H_CA5. In addition, TA12 interferes on H_CA1 interaction with gangliosides. Albeit TA12 prevented H_CA1 binding to GT1b with lower efficiency compared to SV2C-LD, the cumulative effect of TA12 on binding to both types of H_CA1 cell receptors likely contributes to the highly efficient *in vivo* neutralization observed in mouse protection assay. To our knowledge, TA12 is the first antibody able to neutralize BoNT/A by simultaneously interfering with the binding to the two cell surface receptor types on motoneurons.

Acknowledgements

We thank UtechS MSBio of Institut Pasteur for the access to the HDX-MS instrumentation. The CACSICE Equipex ANR-11-EQPX-0008 is acknowledged.

Author contributions

M.R.P. designed the project. S.B., M.R.P, CRE, AW, SS, MM, designed and performed the experiments. S.B., M.R.P and CRE analyzed the data. S.B. and M.R.P. wrote the manuscript. All authors discussed and commented on the manuscript.

533

534 **REFERENCES**

535

536 1. Peck, M. W., Smith, T. J., Anniballi, F., Austin, J. W., Bano, L., Bradshaw, M., Cuervo,
537 P., Cheng, L. W., Derman, Y., Dorner, B. G., Fisher, A., Hill, K. K., Kalb, S. R.,
538 Korkeala, H., Lindstrom, M., Lista, F., Luquez, C., Mazuet, C., Pirazzini, M., Popoff, M.
539 R., Rossetto, O., Rummel, A., Sesardic, D., Singh, B. R., and Stringer, S. C. (2017)
540 Historical Perspectives and Guidelines for Botulinum Neurotoxin Subtype Nomenclature.
541 *Toxins (Basel)* **9**, 38
542 2. Poulain, B., and Popoff, M. R. (2019) Why Are Botulinum Neurotoxin-Producing
543 Bacteria So Diverse and Botulinum Neurotoxins So Toxic? *Toxins (Basel).* **11(1).**
544 toxins11010034. doi: 11010010.11013390/toxins11010034.
545 3. Arnon, S. S., Schechter, R., Inglesby, T. V., Henderson, D. A., Bartlett, J. G., Ascher, M.
546 S., Eitzen, E., Fine, A. D., Hauer, J., Layton, M., Lillibridge, S., Osterholm, M. T.,
547 O'Toole, T., Parker, G., Perl, T. M., Russell, P. K., Swerdlow, D. L., and Tonat, K.
548 (2001) Botulinum toxin as a biological weapon: medical and public health management.
549 *JAMA* **285**, 1059-1070
550 4. Poulain, B., Molgo, J., and Popoff, M. R. (2015) Clostridial neurotoxins: from the
551 cellular and molecular mode of action to their therapeutic use. In *The Comprehensive*
552 *Sourcebook of Bacterial Protein Toxins* (Alouf, J., Ladant, D., and Popoff, M. R., eds)
553 pp. 287-336, Elsevier, Amsterdam
554 5. Rossetto, O., Pirazzini, M., and Montecucco, C. (2014) Botulinum neurotoxins: genetic,
555 structural and mechanistic insights. *Nat Rev Microbiol.* **12**, 535-549. doi:
556 510.1038/nrmicro3295.
557 6. Benoit, R. M., Frey, D., Hilbert, M., Kevenaar, J. T., Wieser, M. M., Stirnimann, C. U.,
558 McMillan, D., Ceska, T., Lebon, F., Jaussi, R., Steinmetz, M. O., Schertler, G. F.,
559 Hoogenraad, C. C., Capitani, G., and Kammerer, R. A. (2014) Structural basis for
560 recognition of synaptic vesicle protein 2C by botulinum neurotoxin A. *Nature.* **505**, 108-
561 111. doi: 110.1038/nature12732.
562 7. Dong, M., Liu, H., Tepp, W. H., Johnson, E. A., Janz, R., and Chapman, E. R. (2008)
563 Glycosylated SV2A and SV2B mediate the entry of botulinum neurotoxin E into neurons.
564 *Mol Biol Cell* **19**, 5226-5237

8. Mahrhold, S., Rummel, A., Bigalke, H., Davletov, B., and Binz, T. (2006) The synaptic vesicle protein 2C mediates the uptake of botulinum neurotoxin A into phrenic nerves. *FEBS Lett* **580**, 2011-2014
9. Rummel, A., Mahrhold, S., Bigalke, H., and Binz, T. (2004) The H_{cc}-domain of botulinum neurotoxins A and B exhibits a singular ganglioside binding site displaying serotype specific carbohydrate interaction. *Mol. Microbiol.* **51**, 631-643
10. Yao, G., Zhang, S., Mahrhold, S., Lam, K. H., Stern, D., Bagramyan, K., Perry, K., Kalkum, M., Rummel, A., Dong, M., and Jin, R. (2016) N-linked glycosylation of SV2 is required for binding and uptake of botulinum neurotoxin A. *Nat Struct Mol Biol* **23**, 656-662
11. Yowler, B. C., Kensinger, R. D., and Schengrund, C. L. (2002) Botulinum neurotoxin A activity is dependent upon the presence of specific gangliosides in neuroblastoma cells expressing synaptotagmin I. *J. Biol. Chem.* **277**, 32815-32819
12. Black, R. E., and Gunn, R. A. (1980) Hypersensitivity reactions associated with botulinal antitoxin. *Am J Med.* **69**, 567-570. doi: 510.1016/0002-9343(1080)90469-90466.
13. Schussler, E., Sobel, J., Hsu, J., Yu, P., Meaney-Delman, D., Grammer, L. C., 3rd, and Nowak-Wegrzyn, A. (2017) Workgroup Report by the Joint Task Force Involving American Academy of Allergy, Asthma & Immunology (AAAAI); Food Allergy, Anaphylaxis, Dermatology and Drug Allergy (FADDA) (Adverse Reactions to Foods Committee and Adverse Reactions to Drugs, Biologicals, and Latex Committee); and the Centers for Disease Control and Prevention Botulism Clinical Treatment Guidelines Workgroup-Allergic Reactions to Botulinum Antitoxin: A Systematic Review. *Clin Infect Dis.* **66**, S65-S72. doi: 10.1093/cid/cix1827.
14. Arnon, S. S., Schechter, R., Maslanka, S. E., Jewell, N. P., and Hatheway, C. L. (2006) Human botulism immune globulin for the treatment of infant botulism. *N Engl J Med* **354**, 462-471
15. Khouri, J. M., Motter, R. N., and Arnon, S. S. (2018) Safety and immunogenicity of investigational recombinant botulinum vaccine, rBV A/B, in volunteers with pre-existing botulinum toxoid immunity. *Vaccine.* **36**, 2041-2048. doi: 2010.1016/j.vaccine.2018.2002.2042.
16. Nayak, S. U., Griffiss, J. M., McKenzie, R., Fuchs, E. J., Jurao, R. A., An, A. T., Ahene, A., Tomic, M., Hendrix, C. W., and Zenilman, J. M. (2014) Safety and pharmacokinetics of XOMA 3AB, a novel mixture of three monoclonal antibodies against botulinum toxin A. *Antimicrob Agents Chemother.* **58**, 5047-5053. doi: 5010.1128/AAC.02830-02814.

17. Rasetti-Escargueil, C., Avril, A., Miethe, S., Mazuet, C., Derman, Y., Selby, K., Thullier, P., Pelat, T., Urbain, R., Fontayne, A., Korkeala, H., Sesardic, D., Hust, M., and Popoff, M. R. (2017) The European AntibotABE Framework Program and Its Update: Development of Innovative Botulinum Antibodies. *Toxins (Basel)* **9,** 309. doi: 10.3390/toxins9100309
18. Lou, J., and Marks, J. D. (2018) Botulinum Neurotoxins (BoNTs)-Antibody and Vaccine. *Toxins (Basel).* **10(12).** toxins10120495. doi: 10120410.10123390/toxins10120495.
19. Fan, Y., Garcia-Rodriguez, C., Lou, J., Wen, W., Conrad, F., Zhai, W., Smith, T. J., Smith, L. A., and Marks, J. D. (2017) A three monoclonal antibody combination potently neutralizes multiple botulinum neurotoxin serotype F subtypes. *PLoS One* **12**, e0174187
20. Garcia-Rodriguez, C., Razai, A., Geren, I. N., Lou, J., Conrad, F., Wen, W. H., Farr-Jones, S., Smith, T. J., Brown, J. L., Skerry, J. C., Smith, L. A., and Marks, J. D. (2018) A Three Monoclonal Antibody Combination Potently Neutralizes Multiple Botulinum Neurotoxin Serotype E Subtypes. Toxins (Basel) 10, doi: 10.3390/toxins10030105
21. Nowakowski, A., Wang, C., Powers, D. B., Amersdorfer, P., Smith, T. J., Montgomery, V. A., Sheridan, R., Blake, R., Smith, L. A., and Marks, J. D. (2002) Potent neutralization of botulinum neurotoxin by recombinant oligoclonal antibody. *Proc. Ntl. Acad. Sci. (USA)* **99**, 11346-11350
22. Lou, J., Wen, W., Conrad, F., Meng, Q., Dong, J., Sun, Z., Garcia-Rodriguez, C., Farr-Jones, S., Cheng, L. W., Henderson, T. D., Brown, J. L., Smith, T. J., Smith, L. A., Cormier, A., and Marks, J. D. (2018) A Single Tri-Epitopic Antibody Virtually Recapitulates the Potency of a Combination of Three Monoclonal Antibodies in Neutralization of Botulinum Neurotoxin Serotype A. *Toxins (Basel)* **10**, 84. doi: 10.3390/toxins10020084
23. Mazuet, C., Dano, J., Popoff, M. R., Creminon, C., and Volland, H. (2010) Characterization of botulinum neurotoxin type A neutralizing monoclonal antibodies and influence of their half-lives on therapeutic activity. *PLoS One* **5**, e12416
24. Prigent, J., Mazuet, C., Boquet, D., Lamourette, P., Volland, H., Popoff, M. R., Creminon, C., and Simon, S. (2010) Production and characterisation of a neutralising chimeric antibody against botulinum neurotoxin A. *PLoS One* **5**, e13245
25. Brier, S., Le Mignon, M., Jain, K., Lebrun, C., Peurois, F., Kellenberger, C., Bordas-Le Floch, V., Mascarell, L., Nony, E., and Moingeon, P. (2018) Characterization of epitope specificities of reference antibodies used for the quantification of the birch pollen allergen Bet v 1. *Allergy.* **73**, 1032-1040. doi: 1010.1111/all.13364.

633 26. Brier, S., Lemaire, D., DeBonis, S., Kozielski, F., and Forest, E. (2006) Use of
634 hydrogen/deuterium exchange mass spectrometry and mutagenesis as a tool to identify
635 the binding region of inhibitors targeting the human mitotic kinesin Eg5. *Rapid Commun*
636 *Mass Spectrom* **20**, 456-462. doi: 410.1002/rcm.2329.
637 27. Volland, H., Lamourette, P., Nevers, M. C., Mazuet, C., Ezan, E., Neuburger, L. M.,
638 Popoff, M., and Creminon, C. (2008) A sensitive sandwich enzyme immunoassay for free
639 or complexed *Clostridium botulinum* neurotoxin type A. *J Immunol Methods* **330**, 120-
640 129
641 28. Tavallaie, M., Chenal, A., Gillet, D., Pereira, Y., Manich, M., Gibert, M., Raffestin, S.,
642 Popoff, M. R., and Marvaud, J. C. (2004) Interaction between the two subdomains of the
643 C-terminal part of the botulinum neurotoxin A is essential for the generation of protective
644 antibodies. *FEBS Lett.* **572**, 299-306
645 29. Couesnon, A., Molgo, J., Connan, C., and Popoff, M. R. (2012) Preferential entry of
646 botulinum neurotoxin A Hc domain trhough intestinal crypt cells and targeting to
647 cholinergic neurons of the mouse intestine. *PLoS Pathog* **8**, e1002583
648 30. Burns, J. R., Lambert, G. S., and Baldwin, M. R. (2017) Insights into the Mechanisms by
649 Which Clostridial Neurotoxins Discriminate between Gangliosides. *Biochemistry.* **56**,
650 2571-2583. doi: 2510.1021/acs.biochem.2576b01246.
651 31. Karalewitz, A. P., Kroken, A. R., Fu, Z., Baldwin, M. R., Kim, J. J., and Barbieri, J. T.
652 (2010) Identification of a unique ganglioside binding loop within botulinum neurotoxins
653 C and D-SA. *Biochemistry* **49**, 8117-8126
654 32. Strotmeier, J., Gu, S., Jutzi, S., Mahrhold, S., Zhou, J., Pich, A., Eichner, T., Bigalke, H.,
655 Rummel, A., Jin, R., and Binz, T. (2011) The biological activity of botulinum neurotoxin
656 type C is dependent upon novel types of ganglioside binding sites. *Mol Microbiol* **81**,
657 143-156
658 33. Malizio, C. J., Goodnough, M. C., and Johnson, E. A. (2000) Purification of *Clostridium*
659 *botulinum* type A neurotoxin. *Methods Mol Biol* **145**, 27-39
660 34. Rasetti-Escargueil, C., Avril, A., Chahboun, S., Tierney, R., Bak, N., Miethe, S., Mazuet,
661 C., Popoff, M. R., Thullier, P., Hust, M., Pelat, T., and Sesardic, D. (2015) Development
662 of human-like scFv-Fc antibodies neutralizing Botulinum toxin serotype B. *MAbs* **7**,
663 1161-1177
664 35. Masson, G. R., Burke, J. E., Ahn, N. G., Anand, G. S., Borchers, C., Brier, S., Bou-Assaf,
665 G. M., Engen, J. R., Englander, S. W., Faber, J., Garlish, R., Griffin, P. R., Gross, M. L.,
666 Guttman, M., Hamuro, Y., Heck, A. J. R., Houde, D., Iacob, R. E., Jorgensen, T. J. D.,

667 Kaltashov, I. A., Klinman, J. P., Konermann, L., Man, P., Mayne, L., Pascal, B. D.,
668 Reichmann, D., Skehel, M., Snijder, J., Strutzenberg, T. S., Underbakke, E. S., Wagner,
669 C., Wales, T. E., Walters, B. T., Weis, D. D., Wilson, D. J., Wintrode, P. L., Zhang, Z.,
670 Zheng, J., Schriemer, D. C., and Rand, K. D. (2019) Recommendations for performing,
671 interpreting and reporting hydrogen deuterium exchange mass spectrometry (HDX-MS)
672 experiments. *Nat Methods.* **16**, 595-602. doi: 510.1038/s41592-41019-40459-y.
673 36. Hourdel, V., Volant, S., O'Brien, D. P., Chenal, A., Chamot-Rooke, J., Dillies, M. A., and
674 Brier, S. (2016) MEMHDX: an interactive tool to expedite the statistical validation and
675 visualization of large HDX-MS datasets. *Bioinformatics.* **32**, 3413-3419. doi:
676 3410.1093/bioinformatics/btw3420. Epub 2016 Jul 3413.
677 37. Guttman, M., Weis, D. D., Engen, J. R., and Lee, K. K. (2013) Analysis of overlapped
678 and noisy hydrogen/deuterium exchange mass spectra. *J Am Soc Mass Spectrom.* **24**,
679 1906-1912. doi: 1910.1007/s13361-13013-10727-13365.
680 38. Pellett, S., Tepp, W. H., Whitemarsh, R. C., Bradshaw, M., and Johnson, E. A. (2015) In
681 vivo onset and duration of action varies for botulinum neurotoxin A subtypes 1-5.
682 *Toxicon* **107**, 37-42
683 39. Whitemarsh, R. C., Tepp, W. H., Bradshaw, M., Lin, G., Pier, C. L., Scherf, J. M.,
684 Johnson, E. A., and Pellett, S. (2013) Characterization of botulinum neurotoxin A
685 subtypes 1 through 5 by investigation of activities in mice, in neuronal cell cultures, and
686 in vitro. *Infect Immun.* **81**, 3894-3902. doi: 3810.1128/IAI.00536-00513.
687 40. Stenmark, P., Dupuy, J., Imamura, A., Kiso, M., and Stevens, R. C. (2008) Crystal
688 structure of botulinum neurotoxin type A in complex with the cell surface co-receptor
689 GT1b-insight into the toxin-neuron interaction. *PLoS Pathog* **4**, e1000129
690 41. Guttman, M., Wales, T. E., Whittington, D., Engen, J. R., Brown, J. M., and Lee, K. K.
691 (2016) Tuning a High Transmission Ion Guide to Prevent Gas-Phase Proton Exchange
692 During H/D Exchange MS Analysis. *J Am Soc Mass Spectrom.* **27**, 662-668. doi:
693 610.1007/s13361-13015-11330-13368.
694 42. Mukherjee, J., Tremblay, J. M., Leysath, C. E., Ofori, K., Baldwin, K., Feng, X.,
695 Bedenice, D., Webb, R. P., Wright, P. M., Smith, L. A., Tzipori, S., and Shoemaker, C.
696 B. (2012) A novel strategy for development of recombinant antitoxin therapeutics tested
697 in a mouse botulism model. *PLoS One* **7**, e29941. doi:
698 29910.21371/journal.pone.0029941.

43. Yao, G., Lam, K. H., Weisemann, J., Peng, L., Krez, N., Perry, K., Shoemaker, C. B., Dong, M., Rummel, A., and Jin, R. (2017) A camelid single-domain antibody neutralizes botulinum neurotoxin A by blocking host receptor binding. *Sci Rep* **7**, 7438
44. Garcia-Rodriguez, C., Geren, I. N., Lou, J., Conrad, F., Forsyth, C., Wen, W., Chakraborti, S., Zao, H., Manzanarez, G., Smith, T. J., Brown, J., Tepp, W. H., Liu, N., Wijesuriya, S., Tomic, M. T., Johnson, E. A., Smith, L. A., and Marks, J. D. (2011) Neutralizing human monoclonal antibodies binding multiple serotypes of botulinum neurotoxin. *Protein Eng Des Sel.* **24**, 321-331. doi: 310.1093/protein/gzq1111.
45. Garcia-Rodriguez, C., Levy, R., Arndt, J. W., Forsyth, C. M., Razai, A., Lou, J., Geren, I., Stevens, R. C., and Marks, J. D. (2007) Molecular evolution of antibody cross-reactivity for two subtypes of type A botulinum neurotoxin. *Nat Biotechnol.* **25**, 107-116. doi: 110.1038/nbt1269.
46. Dong, M., Yeh, F., Tepp, W. H., Dean, C., Johnson, E. A., Janz, R., and Chapman, E. R. (2006) SV2 Is the Protein Receptor for Botulinum Neurotoxin A. *Science* **312**, 592-596
47. Kozaki, S., Kamata, Y., Watarai, S., Nishiki, T., and Mochida, S. (1998) Ganglioside GT1b as a complementary receptor component for *Clostridium botulinum* neurotoxins. *Microbiol. Pathol.* **25**, 91-99
48. Yowler, B. C., and Schengrund, C. L. (2004) Botulinum neurotoxin A changes conformation upon binding to ganglioside GT1b. *Biochemistry* **43**, 9725-9731
49. Hifumi, T., Yamamoto, A., Ato, M., Sawabe, K., Morokuma, K., Morine, N., Kondo, Y., Noda, E., Sakai, A., Takahashi, J., and Umezawa, K. (2017) Clinical Serum Therapy: Benefits, Cautions, and Potential Applications. *Keio J Med.* **66**, 57-64. doi: 10.2302/kjm.2016-0017-IR.
50. Thanongsaksrikul, J., and Chaicumpa, W. (2011) Botulinum neurotoxins and botulism: a novel therapeutic approach. *Toxins (Basel).* **3**, 469-488. doi: 410.3390/toxins3050469. Epub 3052011 May 3050413.
51. Hill, S. E., Iqbal, R., Cadiz, C. L., and Le, J. (2013) Foodborne botulism treated with heptavalent botulism antitoxin. *Ann Pharmacother.* **47**, e12. doi: 10.1345/aph.1341R1646.
52. Hibbs, R. G., Weber, J. T., Corwin, A., Allos, B. M., Abd el Rehim, M. S., Sharkawy, S. E., Sarn, J. E., and McKee, K. T., Jr. (1996) Experience with the use of an investigational F(ab')2 heptavalent botulism immune globulin of equine origin during an outbreak of type E botulism in Egypt. *Clin Infect Dis* **23**, 337-340

732 53. Yu, P. A., Lin, N. H., Mahon, B. E., Sobel, J., Yu, Y., Mody, R. K., Gu, W., Clements, J.,
733 Kim, H. J., and Rao, A. K. (2017) Safety and Improved Clinical Outcomes in Patients
734 Treated With New Equine-Derived Heptavalent Botulinum Antitoxin. *Clin Infect Dis.* **66**,
735 S57-S64. doi: 10.1093/cid/cix1816.
736 54. Marks, J. D. (2004) Deciphering antibody properties that lead to potent botulinum
737 neurotoxin neutralization. *Mov Disord* **19 Suppl 8**, S101-108
738 55. Carter, A. T., and Peck, M. W. (2015) Genomes, neurotoxins and biology of *Clostridium*
739 *botulinum* Group I and Group II. *Res Microbiol* **166**, 303-317
740 56. Mazuet, C., Legeay, C., Sautereau, J., Ma, L., Bouchier, C., Bouvet, P., and Popoff, M.
741 R. (2016) Diversity of Group I and II *Clostridium botulinum* Strains from France
742 Including Recently Identified Subtypes. *Genome Biol Evol* **8**, 1643-1660
743 57. Williamson, C. H., Sahl, J. W., Smith, T. J., Xie, G., Foley, B. T., Smith, L. A.,
744 Fernandez, R. A., Lindstrom, M., Korkeala, H., Keim, P., Foster, J., and Hill, K. (2016)
745 Comparative genomic analyses reveal broad diversity in botulinum-toxin-producing
746 Clostridia. *BMC Genomics* **17**, 180
747

748 **FIGURE LEGENDS**

749

750 **Figure 1 | Effects of TA12 binding on the deuterium uptake behavior of H_CA1**. **A**, The
751 fractional uptake difference plot was generated for each peptide and at each time point by
752 subtracting the deuterium uptake values in the TA12-unbound from those in the bound state.
753 Positive numbers indicate TA12-induced protection (regions 1, 2, 4, 5 and 6) while negative
754 values indicate an increase in solvent accessibility (region 3). The six regions displaying
755 statistically significant changes of deuterium uptake upon TA12 binding (Wald test, $p<0.05$)
756 are highlighted in gray. Each dot corresponds to an average of three independent replicates. **B**,
757 Mapping of the HDX-MS results obtained after 60 min labeling onto the cartoon and surface
758 representations of H_CA1 (pdb # 2NZ9). The largest reductions of deuterium uptake mainly
759 occur within loops (regions 2, 4 and 5) located at the interface between the N-terminal lectin
760 subdomain (H_{CN}) and the C-terminal trefoil subdomain (H_{CC}) whereas changes in dynamics are
761 observed in H_{CN} *only*. "No change" refers to regions of H_CA1 that show no statistically
762 significant uptake difference between states during the time scale of the experiment. **C**, Mass
763 spectra and deuterium uptake plot of peptide 1017-1035 that displays a bimodal isotopic pattern
764 (EX1) in the presence of TA12. The EX1 behavior is characterized by an increase in the peak
765 width due to the overlap of two distinct isotopic distributions corresponding to the low (red)
766 and high (green) *m/z* populations. The center of these two distributions (blue, mix *m/z*) was
767 used to generate the fractional uptake difference values for peptide 1017-1035 (panel A).

768

769 **Figure 2 | TA12 blocks BonT/A1 binding to SV2C-LD by targeting a common area on**
770 **H_CA1. A**, Effects of SV2C-LD binding on the deuterium uptake behavior of H_CA1. The
771 Fractional uptake difference plot was generated for each peptide and at each time point by
772 subtracting the uptake values measured in the SV2C-LD unbound-state from those in the bound
773 state. Positive numbers indicate SV2C-LD induced protection (regions 1, 2, and 3). Regions
774 displaying statistically significant changes of deuterium uptake upon SV2C-LD binding (Wald
775 test, $p<0.05$) are highlighted in gray. Each dot corresponds to an average of three independent
776 replicates. **B**, Mapping of the HDX-MS results obtained after 60 min labeling onto the surface
777 representation of H_CA1 (pdb # 2NZ9). As observed with TA12, the largest reduction in
778 deuterium uptake occurs within region 2 (i.e., 1145-1154 corresponding to region 5 in **Figure**
779 **1A, 1B**). The position of the SV2C-LD binding site identified by X-ray crystallography is also
780 reported (magenta). The H_CA1 residues in direct interaction with SV2C-LD are indicated. "No
781 change" refers to regions of BoNT/A1 that show no statistically significant uptake difference

between states during the time scale of the experiment. **C**, Inhibition of H_CA1 binding to SV2C-LD by mAb TA12. H_CA1 (200 pmol) was preincubated with or without TA12 for 15 min at room temperature (Input) and then incubated with immobilized SV2C-LD on glutathione-Sepharose 4B beads for 90 min at 4°C. Bound H_CA1 was detected by 10% SDS-PAGE analysis after Coomassie blue staining. Load input volumes on gel were 1:10 of the total input volumes. TA12 was dissociated in heavy and light chains. A representative figure of 4 is shown.

Figure 3 | Effects of TA12 on the binding of the GT1b ganglioside. **A**, Structure of the H_CA1:GT1b complexe (pdb # 2VU9) showing the position of the GT1b-binding site relative to the HDX-MS defined TA12 epitope. GT1b is shown as green sticks. A close-up view of the GT1b-binding interface is shown on the right side, where the position of residues Y1117 and F1252 involved in the coordination of GT1b are reported. The GT1b sialic acid 5 (Sia5) and galactose 4 (Gal4) hydrogen bonded respectively to Y1117 and F1252 are also indicated. The variations in deuterium uptake imposed by TA12 binding on H_CA1 are colored as in Figure 1. **B**, TA12 inhibition of H_CA1 binding to GT1b. H_CA1 (10 nM) was preicubated with or without increasing concentration of TA12 for 15 min at room temperature and then exposed to GT1b coated on 96-well plate (1 μg/well). Bound H_CA1 to GT1b was detected with rabbit anti- H_CA1 antibodies and HRP-goat anti-rabbit IgG. Representative experiment in triplicate is shown. TA12 128 nM and above completely prevent the binding of H_CA1 (10 nM) to GT1b.

Figure 4 | TA12 binds H_CA1 on the face opposite occupied by both ciA-C2 and the BoNT/A1-neutralizing therapeutic human monoclonal antibody CR1. Superposition of the structures of the H_CA1:ciA-C2 (pdb # 5L21), H_CA1:CR1 (pdb # 2NYY), H_CA1:GT1b (pdb # 2VU9) and H_CA1:gSV2C (pdb # 5JLV) complexes. GT1b and the N559-glycan of gSV2C are shown as green and cyan sticks respectively. CiA-C2 (dark red) partially occupies the binding site on H_CA1 of both the N-glycan (N559) and the peptide moieties of gSV2C, thereby interfering directly with gSV2C (cyan) binding to H_CA1. The region of H_CA1 containing critical residues for gSV2C binding (i.e., T1145 and T1146) and targeted by ciA-C2 is indicated by a black box. The BoNT/A1-neutralizing CR1 antibody (ribbon representation, gold) directly targets the gSV2C N599-glycan binding site on H_CA1 without competing with the gSV2C peptide binding site (black box). The variable region in the CR1 light chain overalps almost completely with the ciA-C2 binding areas containing the gSV2C N599-glycan interaction site. The HDX-defined TA12 epitope (see color code in Figure 1) occupies the gSV2C peptide binding site targeted by ciA-C2 (black box), causing direct interferences with the peptide

816 moieties of gSV2C. In contrast to both ciA-C2 and CR1, TA12 does not affect the gSV2C
817 glycan binding region but recognize a region of the GT1b-binding site. Thus, TA12 partially
818 impaired $H_cA1$binding to GT1b (Fig. 3B). The position of the TA12 epitope relative to the ciA-
819 C2, CR1 and gSV2C binding sites is better visualized using the H_CA1 surface representation
820 shown on the right side. TA12 shares a common binding interface with cia-C2 but mainly
821 occupies the face opposite on H_CA1 to both ciA-C2 and CR1 (black circle). The position of the
822 N1006 residue identified as important for TA12 binding is indicated.
823
824
825

826 **Table 1**. Neutralization activity of TA12 mAb with BoNT/A subtypes
827
828

TA12 mAb quantity (ng/mouse)	0	10,000	2,500	1,000	250	25	2.5	mAb quantity (ng/mouse) yielding 50% neutralization
BoNT/A1	6/6	0/2	/	0/4	1/7	4/10	6/6	2.5<25
BoNT/A2*	9/9	/	0/9	/	6/9	9/9	/	250
BoNT/A3*	9/9	/	0/9	/	0/9	6/9	/	25<250
BoNT/A5	6/6	5/8	4/4	8/8	5/5	2/2	/	1,000<10,000
BoNT/A7	6/6	1/6	5/6	5/8	8/8	2/2	/	250<1,000

829
830
831 mAb neutralization activity was determined using the mouse protection assay with estimated
832 5 MLD_{50}/mL of BoNT/A subtype and serial dilutions of mAb. 5 estimated MLD_{50}/mouse
833 were incubated with 2.5 to 10,000 ng of TA12 mAb for 30 min at room temperature and the
834 mixture (0.5 mL) was injected intraperitoneally into each mouse.
835 Results are expressed as the number of dead mice versus the total number of mice.
836 *Data from (23).
837

838 **Table 2.** Binding affinities of mAb TA12 with BoNT/A subtypes H_C

839

BoNT/A H_C	Amino acid identity[a] (%)	k_{on} (1/Ms)	k_{off} (1/s)	K_D (pM)
H_CA1	-	$3.01\ 10^5$	$7.1\ 10^{-6}$	23.6
H_CA2	87.0	$6.96\ 10^5$	$7.74\ 10^{-5}$	111
H_CA3	86.58	$1.13\ 10^6$	$6.58\ 10^{-5}$	58.1
H_CA4	91.76	$2.13\ 10^5$	$5.91\ 10^{-4}$	2780
H_CA5	94.11	$7.95\ 10^5$	$7.55\ 10^{-4}$	949
H_CA7	91.76	$2.83\ 10^5$	$5.94\ 10^{-4}$	2100
H_CA1 R1156M		$4.79\ 10^5$	$1.47\ 10^{-5}$	30.7
H_CA1 V1143I/M1144V		$6.42\ 10^5$	$5.63\ 10^{-6}$	8.77
H_CA1 V1143I/M1144V/R1156M		$4.09\ 10^5$	$4.61\ 10^{-5}$	113
H_CA1 N1006A		$1.88\ 10^5$	$1.27\ 10^{-3}$	6755

840

841 [a] Amino acid identity between H_CA1 and the other H_CA subtypes

842

843

844

Figure 1

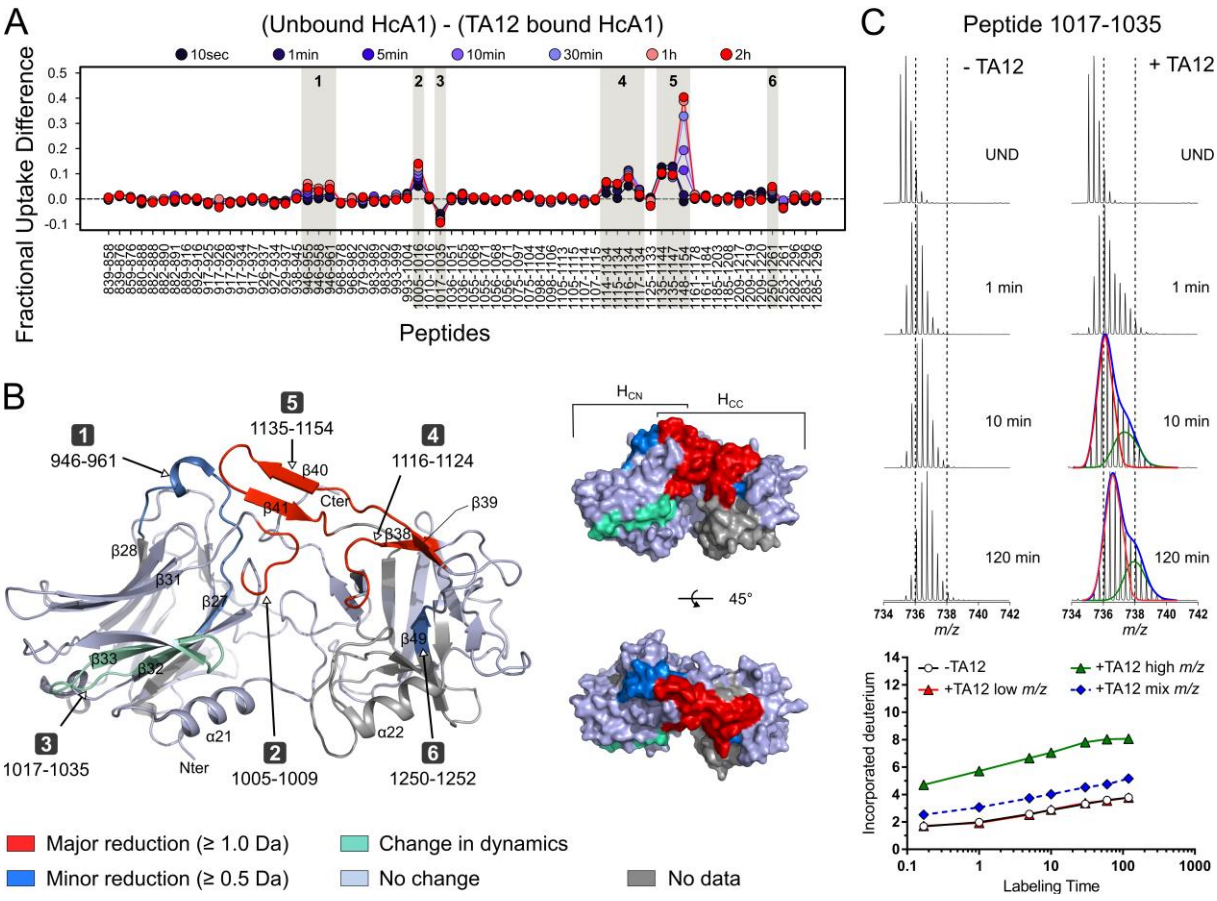
A
(Unbound HcA1) - (TA12 bound HcA1)
10sec
1min
5min
10min
30min
1h
2h
Fractional Uptake Difference
Peptides
B
946-961
1135-1154
1116-1124
1017-1035
1005-1009
1250-1252
Nter
Cter
Major reduction (≥ 1.0 Da)
Minor reduction (≥ 0.5 Da)
Change in dynamics
No change
No data
45°
C
Peptide 1017-1035
- TA12
+ TA12
UND
1 min
10 min
120 min
m/z
-TA12
+TA12 high m/z
+TA12 low m/z
+TA12 mix m/z
Incorporated deuterium
Labeling Time

Figure 2

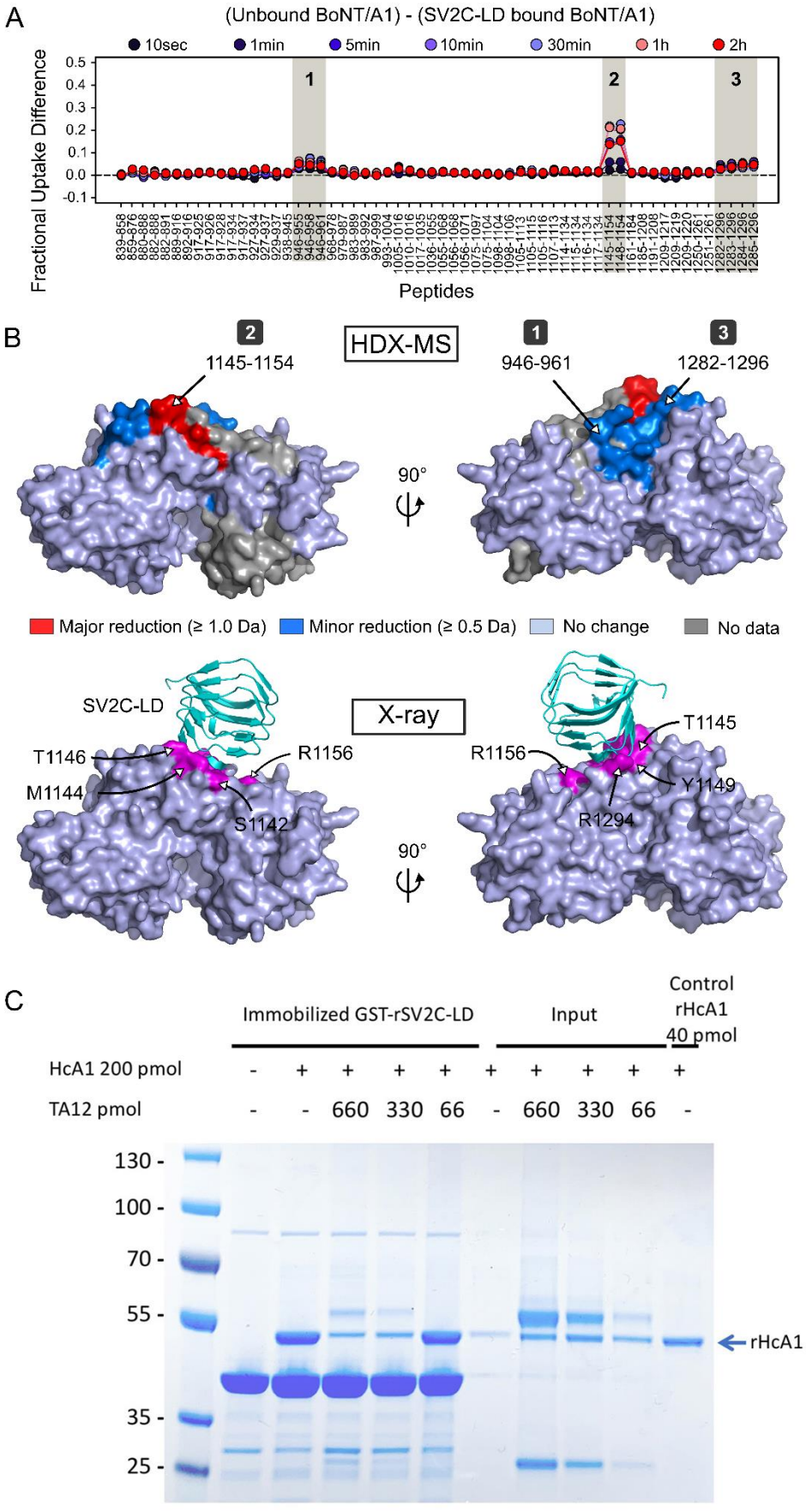
A
(Unbound BoNT/A1) - (SV2C-LD bound BoNT/A1)
10sec
1min
5min
10min
30min
1h
2h
Fractional Uptake Difference
Peptides
B
HDX-MS
1145-1154
946-961
1282-1296
90°
Major reduction (≥ 1.0 Da)
Minor reduction (≥ 0.5 Da)
No change
No data
SV2C-LD
X-ray
T1146
R1156
M1144
S1142
T1145
Y1149
R1294
C
Immobilized GST-rSV2C-LD
Input
Control rHcA1 40 pmol
HcA1 200 pmol
TA12 pmol
130 -
100 -
70 -
55 -
35 -
25 -
rHcA1

851

852 **Figure 3**
853

A

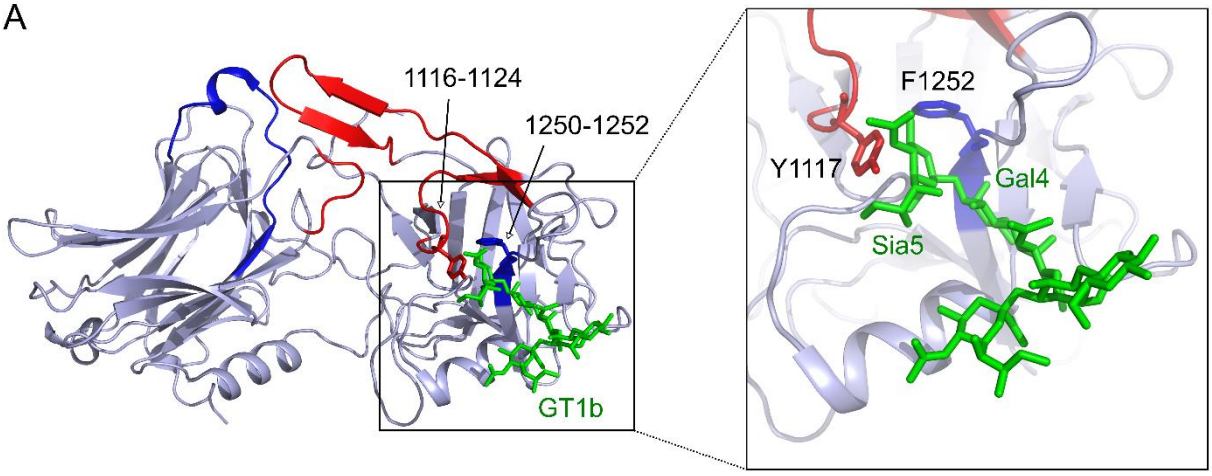

B

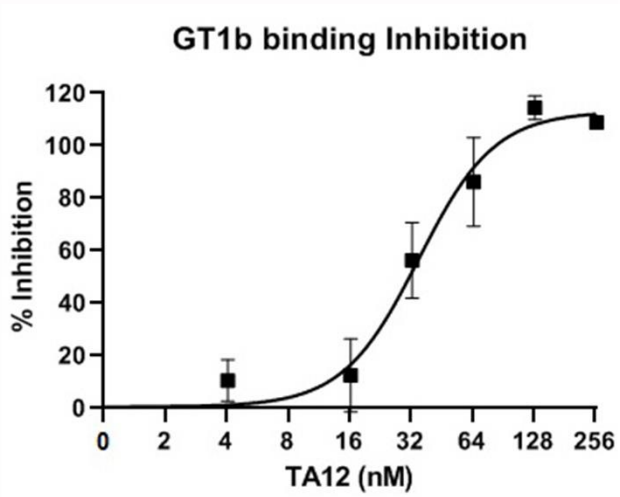

854

855 **Figure 4**
856

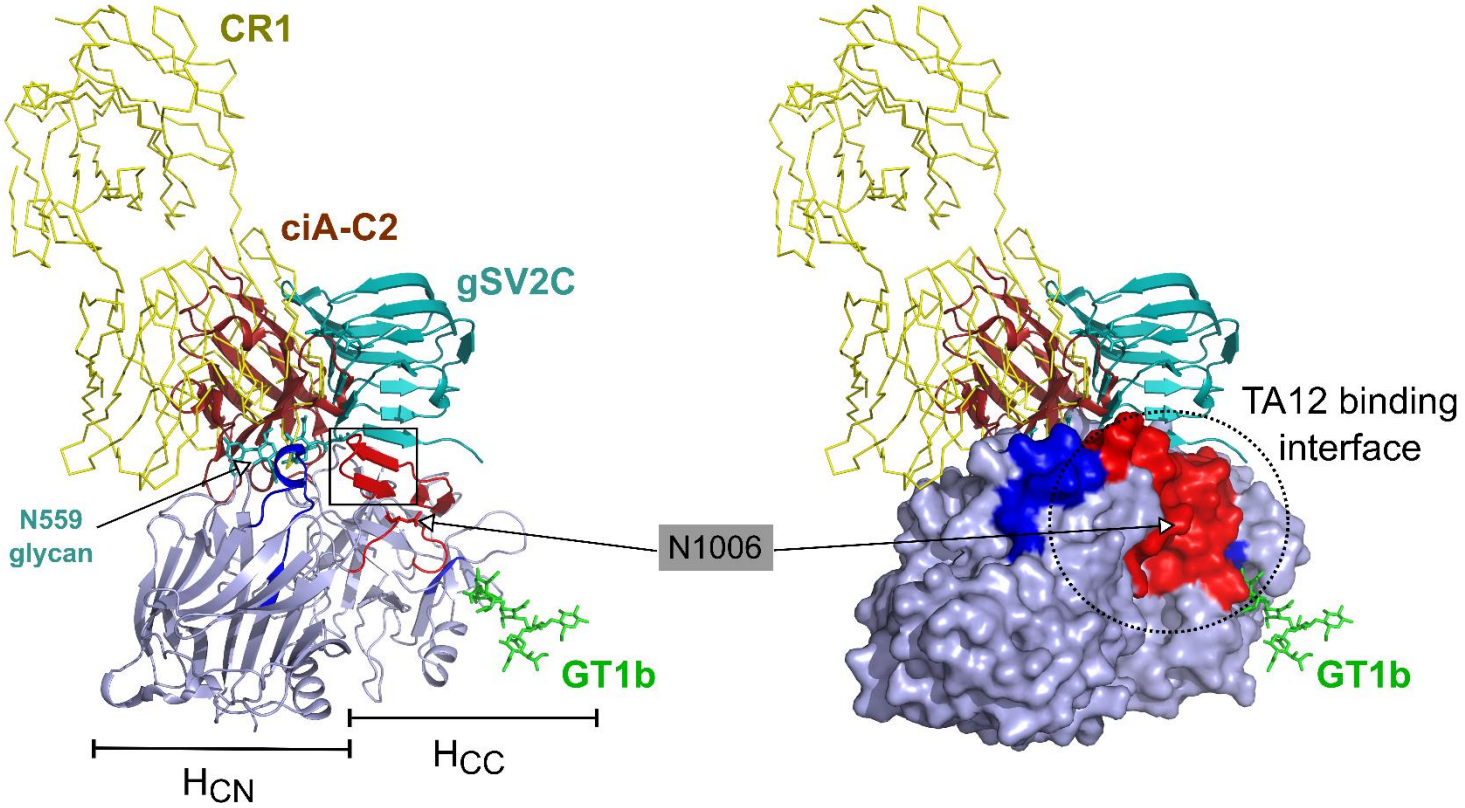

857